

# The demise of the synchronous moon that gave Mars its triaxiality. The role of solar tides and a palaeo ocean

Michael Efroimsky

US Naval Observatory, Washington DC 20392 USA

michael.efroimsky@gmail.com

## Abstract

Mars' asymmetric figure — with two opposing equatorial elevations — stemmed from a frozen tidal bulge raised by a primordial synchronous moon Nerio. Nerio's emergence, through *in situ* formation or by capture in the disk's remnants, and its synchronisation with Mars' rotation preceded or coincided with crust formation. The submoon and antimoon regions hypothetically developed thinner crusts, intensifying tectonics that amplified Mars' triaxiality. We investigate Nerio's orbit stability and demise, and its impact on Mars' rotation. The synchronous orbit is stable transiently: solar tides adiabatically shrink it, accelerating Mars' rotation. This evolution proceeds gradually, so Mars' tidal bulge freezes. Following the LHB water delivery and ocean formation, solar tides intensify, making Nerio's synchronous orbit unstable. Nerio departs synchronism and spirals down, accelerating Mars' spin. Mars' angular velocity at the desynchronisation moment matches its present-day value to the first decimal place. This coincidence should not be overinterpreted, as post-desynchronisation evolution included Mars' continued spin-up during Nerio's descent (till Nerio's destruction amid the LHB), followed by Mars' despinning by solar tides. Nerio's reaching the Roche limit intact is questionable. Beyond LHB hazards, it would imply Mars' larger spin-up, necessitating  $k_2/Q \simeq 4.7$  to allow subsequent despinning to the present-day rate. Such values may be high even for shallow oceans. Absent future evidence supporting such elevated  $k_2/Q$  values, Nerio likely perished during the LHB. This viewpoint may be reconsidered should new data on Mars' palaeo ocean show up.

## 1 Preliminaries

About 9.3 times less massive than the Earth, Mars has had a very different geological history. It had been losing its internal heat much faster, and its volcanism eventually came to an end. Due to the rapid cooling, Mars has preserved a manifestly nonhydrostatic shape. Highly triaxial and unusually asymmetric for a terrestrial planet, this shape is marked with two large near-equatorial elevations located almost opposite to one another — a highly improbable configuration. One of these uplifts is, of course, the colossal Tharsis Rise (0°N 260°E). The other is a less prominent elevation comprising Elysium Planitia (0°N 80°E), Syrtis Major Planum (8.4°N 69.5°E) and, arguably, an adjacent to Syrtis Major part of Terra Sabaea.

### 1.1 Primordial synchronous moon as a source of Mars' initial asymmetric triaxiality

Positioned on opposite sides of the equator, but differing in mean height, the two aforementioned great elevations are likely to have proven from a fossilised tidal bulge generated by a massive synchronous moon (Efroimsky,

2024). In *Ibid.*, it was also suggested that in the tidally elevated submoon and antimoon areas the subsequent tectonic and volcanic activity became higher, leading to further elevation of those provinces. It was demonstrated there that to cause the initial asymmetric triaxiality of an early Mars, the moon should have a mass

$$M_m \lesssim 0.032 M, \quad (1)$$

$M$  being the mass of Mars. The moon was named *Nerio*, after a female companion of Mars in early Roman mythology.

Nerio ought to have disintegrated sufficiently early, so the resulting latitudinal distribution of craters could then be smeared by the Late Heavy Bombardment (LHB). In this way, having accreted *in situ* simultaneously with Mars, or captured shortly after Mars' formation some 4.6 Gyr ago, the moon should have disappeared by 4 Gyr or, at the latest, 3.8 Gyr ago, given the LHB timing.<sup>1</sup> This lifespan would have been long enough to create a seed triaxiality in the planet and, hypothetically, to result in a thinner crust in the elevated areas, increasing their chances for subsequent tectonic and volcanic rise.

Finally, despite the large chaotic excursions in Mars'

<sup>1</sup> Some authors suggest that the LHB was declining gradually until ~ 3.1 Gyr ago (Hartmann et al., 2007).

obliquity over geological time (Touma and Wisdom, 1993; Laskar and Robutel, 1993), the moon — once captured near the equator — remained tightly coupled to the moving equator, exhibiting only small inclination oscillations.<sup>2</sup>

## 1.2 The moon’s origin and demise

As explained above, Nerio must have emerged during Mars’ earliest history, when the newborn planet was still sufficiently soft and deformable. Along with *in situ* accretion, capture in the remnants of the disk could be a viable option.

For Nerio’s presence to overlap with the era of crustal solidification on Mars — and thereby to allow the tidal bulge to become frozen into the planet’s figure — its synchronous orbit would need to remain stable for a sufficient (though not necessarily perpetual) period of time. While the moon’s eventual destruction can plausibly be attributed to the onset of the LHB, it is worthwhile to investigate, *inter alia*, if Nerio could have reached the Roche limit after its orbit was destabilised by solar tides acting to decelerate Mars’ rotation.

## 1.3 The synchronous radius linked to the time of Nerio’s orbital synchronisation

The synchronous radius  $r$  relates to the planet’s rotation rate  $\Omega$  via

$$r^3 = \frac{G(M + M_m)}{\Omega^2} . \quad (2)$$

The centrifugal force can be decomposed into components — one purely radial, another imitating the axially symmetrical part of a quadrupole tidal perturbation. The former component negligible for incompressible bodies, the latter produces a dynamical oblateness  $J_2$ . Hence a relation connecting  $J_2$  with the rotation rate  $\Omega$  and the quadrupole Love number (see, e.g. Appendix C to Efroimsky 2024):

$$\Omega^2 = \frac{3GMJ_2}{R^3 k_2} , \quad (3)$$

$R$  being the early radius of Mars (different from the present radius by some 0.6% due to the Late Veneer and LHB).

In the former and latter formulae,  $\Omega$  is the planet’s spin rate established at the moment of synchronisation,

<sup>2</sup> For uniform equinoctial precession, this fact was proved by Goldreich (1965) who, as it turned out, carried out his development in nonosculating orbital elements. A later analysis in osculating elements confirmed his conclusion (Efroimsky, 2005). The case of nonuniform variations of the planet’s obliquity required a further study — which established that in this situation, too, a near-equatorial satellite is never repelled considerably from the equator of date (Gurfil et al., 2007).

i.e., equal to the mean motion of the moon at that time. In the absence of solar tides, the value  $\Omega$  would then be sustained by the synchronous moon for as long as it existed. Consequently,  $r$  would remain unchanged through the moon’s lifetime. Solar tides, however, altered the dynamics by applying a torque to the planet. Since the torque was decelerating, one might expect it to have been mitigating Mars’ spin. This indeed is what happens to a planet in the absence of a synchronous moon. In its presence, however, the situation becomes more complex. Quite counterintuitively, solar tides on Mars made the synchronous state adiabatically evolve in the direction of a slow **increase** in  $\Omega$  and, consequently, a slow decrease in  $r$ , as will be shown in Section 3. Here, *slow* has a precise meaning: the said evolution of the synchronous state was **much** slower than the process of Mars’ figure solidification.<sup>3</sup> This enables us to identify the value of  $\Omega$  at the time of Mars’ figure solidification with the value of  $\Omega$  at the time of Nerio’s synchronisation.

Combining equations (2) and (3), we express the synchronous radius’ early value  $r$  through the early values of the Love number and oblateness:

$$\frac{r}{R} = \left( \frac{k_2}{3J_2} \frac{M + M_m}{M} \right)^{1/3} . \quad (4a)$$

Nerio’s life time spanned from 4.6 – 4.5 through, at most, 4.0 – 3.8 Gyr ago. Since the Martian figure solidified before Nerio’s demise, it is reasonable to approximate the then  $J_2$  of Mars with its present value:  $J_2 \approx J_2^{(\text{present})}$ . Also be mindful that  $J_2$  enters the above expression raised to the power of 1/3, which makes  $r$  less sensitive to the uncertainty in the value of  $J_2$ . Formula (4a) therefore becomes:

$$\frac{r}{R} \approx 5.54 \left( 1 + \frac{M_m}{M} \right)^{1/3} k_2^{1/3} . \quad (4b)$$

Through this expression, the synchronous radius at the time of the moon’s synchronisation is linked to the quadrupole Love number value at that time.

The title of this subsection indicates the necessity to express the planet’s synchronous radius and rotation rate as functions of the time of the moon’s orbital synchronisation. This could be accomplished by using equations (4b) and (2), were the time dependence  $k_2(t)$  known.

<sup>3</sup> On the one hand, magma-ocean crystallisation and primordial-crust formation on Mars were extremely rapid, occurring in less than 20 Myr. Even if the crust were reworked by impacts ~ 100 Myr later (as proposed by Bouvier et al. 2018), it remains safe to assume that the Martian figure fossilised within several hundred Myr after the planet’s accretion — certainly well within 0.5 Gyr.

On the other hand, we shall see in Section 5 that prior to the formation of a palaeo ocean on Mars, the tidal response of the Mars-Nerio system to solar tides was weak, rendering the increase in  $\Omega$  and the ensuing possible change in  $J_2$  negligible. The system’s response to solar tides was boosted greatly by the ocean, but this enhancement occurred when Mars was ~ 0.5 Gyr old, its figure long frozen.

Table 1 Symbol key

Variable	Value	Explanation	Reference
$G$	$6.67430 \times 10^{-11} \frac{\text{m}^3}{\text{kg s}^2}$	gravitational constant	Tiesinga et al. (2021)
$M$	$6.31 \times 10^{23} \text{ kg}$	early Mars' mass	Efroimsky (2024, Eqn 15)
$R$	$3.37 \times 10^6 \text{ m}$	early Mars' mean radius	Efroimsky (2024, Eqn 15)
$M^{(\text{present})}$	$6.4169 \times 10^{23} \text{ kg}$	present Mars' mass	Konopliv et al. (2016)
$R^{(\text{present})}$	$3.3895 \times 10^6 \text{ m}$	present Mars' mean radius	Seidelmann and Urban (2013)
$k_2$		early Mars' Love number	
$Q$		early Mars' quality factor	
$K_2 \equiv \frac{k_2}{Q}$		early Mars' quality function	
$r$		early Mars' synchronous radius	Equation (2)
$\dot{\theta}$		Mars' rotation rate	
$\Omega$		early synchronous value of $\dot{\theta}$	Equation (3)
$a$		Nerio's semimajor axis	
$a_M$	$2.2794 \times 10^{11} \text{ m}$	Mars' semimajor axis	
$n$		Nerio's mean motion	
$A < B < C$		early Mars' moments of inertia	
$\xi \equiv \frac{C}{MR^2}$		early Mars' MOI factor	
$\xi^{(\text{present})}$	0.36379	present Mars' MOI factor	Khan et al. (2018)
$J_2$		early Mars' oblateness	$J_2 \equiv \frac{C - (A + B)/2}{MR^2}$
$J_{22}$		early Mars' triaxiality	$J_{22} \equiv \frac{B - A}{4MR^2} = \sqrt{C_{22}^2 + S_{22}^2}$
$J_2^{(\text{present})}$	$1.9566 \times 10^{-3}$	present Mars' oblateness	Konopliv et al. (2011)
$J_{22}^{(\text{present})}$	$6.3106 \times 10^{-5}$	present Mars' triaxiality	Konopliv et al. (2020, Table S4)
$M_m$		Nerio's mass	
$M_\odot$	$2.09 \times 10^{30} \text{ kg}$	early Sun's mass	Appendix A

Finding this time-dependence would, however, amount to a major project focused on modeling the evolution of a *nonspherical* nascent planet. Taking into account the asymmetric shape, the model should specifically account for the change of rheology during the cooling of the young Mars, a process involving in particular the solidification of an early magma ocean, and the formation and thickening of Mars' stagnant lid. To sidestep this major work — and still obtain physically meaningful estimates — the timing question can be tackled through a simpler parameterisation of the solidification process. Following Efroimsky (2024), we are using, instead of time, the evolving mean rigidity  $\mu$  as a parameter through which to express the Love number,  $k_2(\mu)$ . This approach is sound, because the values of  $\mu$  can be reasonably related to the stages of Mars' early history. The mean rigidity grew from  $\approx 0.20$  GPa, at the end of the magma-ocean stage, to  $\approx 18$  GPa at the stage of solidification, see *Ibid.* and references therein:

$$0.20 \text{ GPa} \lesssim \mu \lesssim 18 \text{ GPa} . \quad (5)$$

Under static loading, the Love number is defined by the mean shear rigidity  $\mu$  via the formula

$$k_2 = \frac{3}{2} \frac{1}{1 + \mathcal{B}_2 \mu} , \quad (6)$$

where

$$\mathcal{B}_2 = \frac{57}{8\pi G (\rho R)^2} = 0.193 \times 10^{-9} \text{ kg}^{-1} \text{ m s}^2 , \quad (7)$$

$G$  being the Newton gravitational constant,  $\rho$  being the young Mars' mean density, and  $R$  its mean radius.

Substituting the bounds (5) on  $\mu$  into equation (6), and inserting the result into expression (4b), shows that the values of the synchronous radius are constrained to the interval

$$3.88 \lesssim \frac{r}{R} \lesssim 6.26 . \quad (8)$$

The upper bound on  $r/R$  is appropriate, via equation (4a), to the upper bound on  $k_2$  and therefore, through equation (6), to the lower value  $\mu \approx 0.20$  GPa — which, in its turn, corresponds to a situation where Nerio became synchronous and shaped Mars' figure already at the magma-ocean stage.

The lower bound on  $r/R$  is, on the other hand, defined by the lower bound on  $k_2$  or, equivalently, by the upper value  $\mu \approx 18$  GPa — which is the case of Nerio synchronising its orbit and shaping the planet at the time when Mars' solidification was already going on.

Note that the lower bound on  $r/R$  is well above the Roche limit, which in this case is  $2.32R$  (Efroimsky, 2024, Section 7.1).

In Section 4, we shall see that a different, purely dynamical reasoning imposes a lower bound on  $r/R$  more stringent than in equation (8).

## 2 (In)stability of synchronous orbits

### 2.1 Is a synchronous orbit always stable?

For the first time, this question was addressed yet by Darwin (1879). Later, it was tackled by Counselman (1973) and Hut (1981), whose analysis was probably more mathematically complex than necessary.

To gain intuition, we first approach the problem in elementary terms.

The orbital angular momentum

$$H_{\text{orb}} = \frac{M M_m}{M + M_m} \sqrt{G(M + M_m) a (1 - e^2)} \quad (9)$$

is proportional to a positive power of  $a$ . Therefore, an infinitesimal increase  $\delta a > 0$  of the semimajor axis entails an increase  $\delta H_{\text{orb}} > 0$ . Owing to the conservation law, this yields a decrease in the spin angular momentum of the planet, and therefore a negative change  $\delta \Omega < 0$  of its rotation rate. The synchronous radius

$$r = \left[ \frac{G(M + M_m)}{\Omega^2} \right]^{1/3} \quad (10)$$

of the planet scales as  $\Omega$  to a negative power. Hence  $\delta \Omega < 0$  produces an increase in the synchronous radius,  $\delta r > 0$ . We observe that the infinitesimal variations of  $a$  and  $r$  have the same sign:

$$\delta a > 0 \implies \delta H_{\text{orb}} > 0 \implies \delta \Omega < 0 \implies \delta r > 0 . \quad (11)$$

The configuration is stable if  $\delta r > \delta a$ , because this inequality ensures that an infinitesimal increase in  $a$  leads to a subsequent infinitesimal tidal descent.

Alternatively, if we reverse all signs,

$$\delta a < 0 \implies \delta H_{\text{orb}} < 0 \implies \delta \Omega > 0 \implies \delta r < 0 , \quad (12)$$

the stability condition will imply that a negative  $\delta a$  must produce a negative  $\delta r$  of a larger absolute value, so the moon finds itself above synchronism and performs an infinitesimal tidal ascent.

It can be shown that for fixed values of the primary and secondary masses, a tidal binary can have up to two synchronous spin-orbit configurations. When these configurations are two, one is stable, another not. This was a conclusion to which Darwin (1879), Counselman (1973) and Hut (1981) arrived by various means. We here prefer to link these two possible outcomes to the initial conditions, as was done in Makarov and Efroimsky (2025).

### 2.2 A stability criterion

For a small eccentricity and obliquities and a negligible spin angular momentum of the secondary,

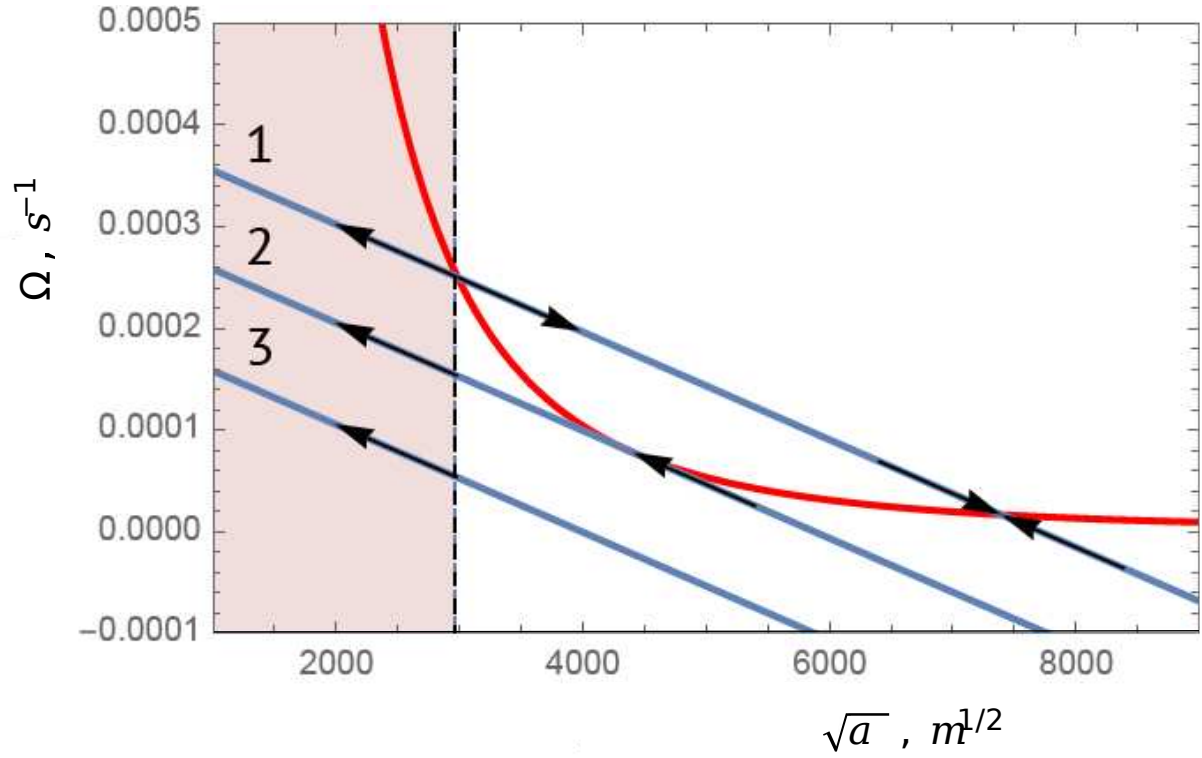


Figure 1 The blue lines **1**, **2**, **3** depict different dynamical tracks given by equation (14) for different sets of initial conditions  $\{a(t_0), \Omega_0\}$ , with the masses' values  $M$  and  $M_m$  fixed. The red cubical hyperbola comprises, for fixed  $M$  and  $M_m$ , all synchronous states given by equation (17). Track **1** crosses the red curve in two points, only one of which is a stable synchronous state, see equation (18b) and the paragraph after it. Track **2** is tangent to the red curve, and shares only one point with it. As demonstrated in Section 3 and Figure 2, this synchronous state is unstable under a perturbation generated by solar tides. Track **3** originates from initial conditions excluding the possibility of synchronism. The vertical dashed line and the beige-shaded area indicate the Roche limit. If the moon is not destroyed by the LHB prior to crossing that limit, it gets disintegrated there by tidal forces.

the angular momentum conservation law yields (Makarov and Efroimsky, 2023, Appendix D):

$$\frac{\dot{\Omega}}{\dot{n}} = \frac{1}{3\xi} \frac{M_m}{M + M_m} \left(\frac{a}{R}\right)^2 + O(e^2), \quad (13)$$

$\xi$  being the moment of inertia (MOI) factor of the primary mass.

Integration of this equation in neglect of  $O(e^2)$ , performed in Makarov and Efroimsky (2025, Section 2), produces

$$\Omega = -X\sqrt{a} + C, \quad (14)$$

with the integration constant given by

$$C = X\sqrt{a(t_0)} + \Omega(t_0) \quad (15)$$

and the slope equal to

$$X = \frac{M_m}{\xi} \sqrt{\frac{G}{M + M_m}} R^{-2}. \quad (16)$$

The value of the slope  $X$  parameterises the angular-momentum exchange rate between the planet's spin and moon's orbit.

We observe that for small eccentricity and obliquities, and in neglect of the spin angular momentum of the moon, each dynamical history makes a linear function in the  $(\sqrt{a}, \Omega)$  coordinates.

The synchronicity condition  $\Omega = n$  can be written down as

$$\Omega = \sqrt{G(M + M_m)} (\sqrt{a})^{-3}, \quad (17)$$

producing a cubical hyperbola in the  $(\sqrt{a}, \Omega)$  coordinates.

These observations are illustrated in Figure 1 where each inclined blue line implements a dynamical history (14) defined by some initial condition  $(\sqrt{a}(t_0), \Omega(t_0))$ . The red curve is the cubical hyperbola (17). The figure explains why for a fixed pair of mass values,  $M$  and  $M_m$ , the number of available synchronous orbits can be zero, or one, or two — depending on the initial conditions.

As we mentioned above, several authors had established, by different methods, that whenever two synchronous states are available, one is stable, another not. We, however, favour a still different approach, which we find not only straightforward but also more general. It comprises two steps. First, approximate the tidal rate  $da/dt$  of the semimajor axis with its quadrupole semidiurnal part  $(da/dt)^{(pqs)}$  caused by the tides in the planet only.<sup>4</sup> Second, take the full (not partial) derivative of  $(da/dt)^{(pqs)}$  over  $a$ , in the synchronous state, i.e., for

$n = \Omega$ . This renders (Makarov and Efroimsky, 2025, Appendix A):

$$\frac{d}{da} \left( \frac{da}{dt} \right)_{n=\Omega}^{(pqs)} = 9 \frac{M_m}{M} \left( \frac{R}{a} \right)^5 n^2 \left( 1 - \frac{d\Omega}{dn} \right) \frac{dK_2(\omega)}{d\omega} \Big|_{\omega=0}, \quad (18a)$$

where  $K_2$  is the quality function, and the shortened notation  $\omega \equiv \omega_{2200} = 2(n - \Omega_p)$  is introduced. For realistic rheologies,  $dK_2(\omega)/d\omega$  at the point  $\omega = 0$  is positive, as was illustrated by the case of a Maxwell planet in *Ibid.* The derivative  $d\Omega/dn$  is given by equation (13) above.

A synchronous spin-orbit state is stable (unstable) when the derivative  $\frac{d}{da} \left( \frac{da}{dt} \right)_{n=\Omega}^{(pqs)}$  is negative (positive). Hence the stability criterion deduced in *Ibid.*:

Synchronism is stable if  $d\Omega/dn > 1$ ; unstable otherwise.

The criterion indicates that for a straight line crossing the cubical curve in Figure 1, the left crossing point is unstable, the right is stable. To understand the reason for this, rewrite expression (18a) as

$$\frac{d}{da} \left( \frac{da}{dt} \right)_{n=\Omega}^{(pqs)} = 9 \frac{M_m}{M} \left( \frac{R}{a} \right)^5 n^2 \left( 1 - \frac{d\Omega/d\sqrt{a}}{dn/d\sqrt{a}} \right) \frac{dK_2(\omega)}{d\omega} \Big|_{\omega=0} \quad (18b)$$

and recall that  $d\Omega/d\sqrt{a}$  and  $dn/d\sqrt{a}$  are the slopes of the straight line and the cubical curve, correspondingly (both slopes being negative). At the left crossing point in Figure 1, the absolute value of the slope of the linear function,  $|d\Omega/d\sqrt{a}|$ , is larger than that of the cubical curve,  $|dn/d\sqrt{a}|$ , so the state is unstable. At the right crossing point, the situation is opposite; hence the stability of that state (assuming that the orbit is located between the Roche and reduced Hill radii).

This criterion from *Ibid.* is more generic than the techniques proposed in the literature thitherto, because the stability analysis based on examining the sign of the derivative  $\frac{d}{da} \left( \frac{da}{dt} \right)_{n=\Omega}$  can be applied to settings incorporating finite eccentricity and obliquities, higher-than-quadrupole terms, tides in the moon, as well as the planet's nonsphericity, the Sun's gravitational pull, and other perturbations. Within this approach, one is free to use an expression for  $\left( \frac{da}{dt} \right)_{n=\Omega}$  to any required precision in the powers of  $e$  and  $i$ , and with any additional physical effects included. A subsequent turn-of-the-crank differentiation over  $a$  provides the result. Furthermore, this method is equally effective for analysing the stability of higher-order spin-orbit resonances, as was demonstrated in Section 4 of Makarov and Efroimsky (2025) where the stability of the 3:2 spin-orbit state was addressed.

<sup>4</sup>The superscript "(pqs)" means: *planet, quadrupole, semidiurnal*.

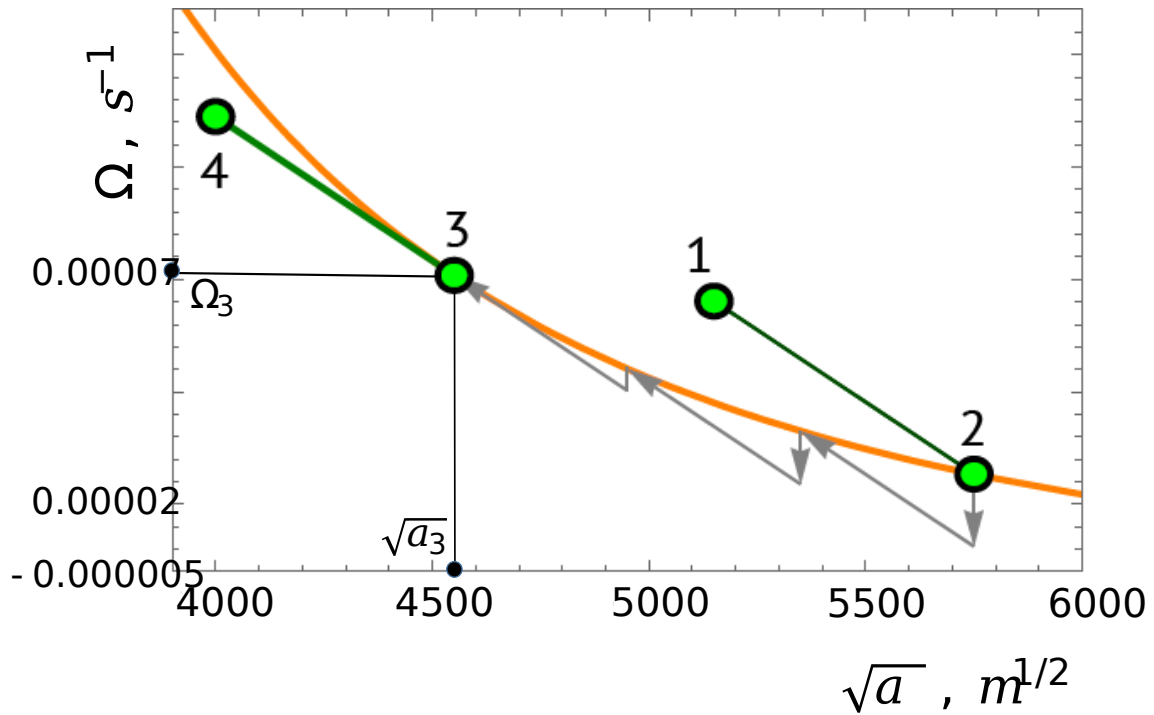


Figure 2 An instantaneous action of solar tides entails an infinitesimal reduction of the planet’s rotation rate, as shown by a short vertical arrow pointed downwards from the stable point of synchronisation 2. This action pushes the system to a different dynamical history terminating at a synchronous state with a slightly smaller  $a$  and a slightly higher  $\Omega = n$ . After numerous pushes, the system arrives at the marginal state 3. That state is unstable, and an infinitesimal action by the solar tides in that state finally sets the system on its final trajectory along which it starts moving towards the Roche limit, point 4. The green disks and connecting lines show a plausible evolution scenario: (1) An initial state where Mars rotates faster than the orbital motion. (2) Capture of Mars into a long-term synchronous equilibrium. (3) The critical point is attained due to the action of solar tides, and Mars is released from the resonance. (4) The satellite is migrating towards the Roche limit, and is likely destroyed by the LHB *en route* thereto.

As an aside (not relevant to Mars, but of general interest),  $\Omega$  may in principle have a negative sign — corresponding to rotation retrograde w.r.t. the mean motion of the moon. In that setting, a moon undergoing inward tidal migration can reverse the planet’s rotation, depending on the initial conditions and the mass ratio (Makarov and Goldin, 2024).

### 3 Solar tides on the planet make the marginal state unstable

Weak yet relentless, solar tides are adiabatically driving an initially stable spin state toward instability (Ward and Reid, 1973; Makarov and Efroimsky, 2025). In Figure 2, each short downward-pointing vertical arrow shows how solar tides slightly slow down the planet’s rotation rate over a brief period. This infinitesimal action pushes the system towards a different dynamical history, a straight line parallel to the initial dynamical track and located slightly to the left of it. Now residing on this new trajectory, the system moves along it towards the new intersection with the cubical hyperbola. This new equilibrium is located on the hyperbola slightly to the left of the preceding equilibrium state. This shifted equilibrium corresponds to a slightly higher value of  $\Omega$  and a slightly smaller synchronous radius  $r$ .

Slowly but steadily, the state of the system is migrating leftwards along the cubical hyperbola, over a set of transiently stable synchronous states. Were it not for the synchronous moon, solar tides would be working to slow down Mars’ rotation. The presence of a synchronous partner, however, results in a slow spin-up. The system eventually arrives at the marginal state depicted with point 3 in Figure 2. In Figure 1, this borderline state is a point where the blue line 2 is tangent to the cubical curve.

The borderline spin state is transiently stable under an infinitesimal increase in the planet’s spin rate  $\Omega$  — but is unstable under a decrease, because a decrease in  $\Omega$  shifts the system to an adjacent trajectory (line 3 in Figure 1) lacking intersection with the cubical curve. Along that new trajectory, the system starts moving leftwards to the Roche radius. Solar tides thus are rendering the marginal state unstable.

In the marginal state, the straight line depicting a physical history is tangent to the cubical curve. Consequently, their slopes are equal:

$$\frac{dn}{d\sqrt{a}} = \frac{d\Omega}{d\sqrt{a}} \iff \frac{d\Omega}{dn} = 1. \quad (19)$$

Combining this with equation (13), we find that the marginal point corresponds to a synchronous orbit of the radius  $r$  satisfying

$$\frac{1}{3\xi} \frac{M_m}{M + M_m} \left(\frac{r}{R}\right)^2 = 1 \iff \frac{r}{R} = \sqrt{3\xi \frac{M + M_m}{M_m}}. \quad (20)$$

For  $M_m$  of order  $0.03M$ , the resulting values of  $r$  come out well above the Roche limit  $r_R = 2.32R$ .

### 4 Constraints on the parameters of the moon

From equation (20) and the stability criterion  $d\Omega/dn > 1$  obtained in Section 2.2, we deduce that the initial synchronous state of the moon must satisfy the condition

$$\frac{r}{R} > \sqrt{3\xi \frac{M + M_m}{M_m}}. \quad (21)$$

Combined with the expression (4a) for  $r/R$ , inequality (21) produces

$$3\xi \left(1 + \frac{M_m}{M}\right)^{1/3} \left(\frac{3J_2}{k_2}\right)^{2/3} < \frac{M_m}{M}. \quad (22)$$

In Efroimsky (2024, Eqn 21), we demonstrated that

$$\frac{M_m}{M} \approx \frac{J_{22}}{J_2}, \quad (23)$$

where  $J_2$  and  $J_{22}$  are Mars’ oblateness and triaxiality at the synchronisation time.

Above, in Section 1.3, we found that the then value of  $J_2$  was not very different from its present value,  $J_2 \approx J_2^{(\text{present})}$ , because the synchronous moon was, during its existence, sustaining the planet’s spin rate — and therefore its shape — until the shape fossilised. If the early fossilisation was not complete, and slight residual adjustment of shape to the tidally decelerating spin continued for some time, the said approximation should be given a more conservative form:

$$J_2 \gtrsim J_2^{(\text{present})}. \quad (24)$$

By distinction, the value of  $J_{22}$  may have slightly increased since then, because the Nerio-generated seed triaxiality could have produced a thinner crust in the submoon and antimoon points, caused higher tectonic activity in those two zones, and leading to greater elevations and, as a result of that, to a further increase in  $J_{22}$ . Therefore,

$$J_{22} \lesssim J_{22}^{(\text{present})}. \quad (25)$$

Owing to inequalities (24) and (25), expression (23) becomes:

$$\frac{M_m}{M} \lesssim \left(\frac{J_{22}}{J_2}\right)^{(\text{present})}. \quad (26)$$

In combination with inequality (21), it yields the interval

$$3\xi \left(1 + \frac{M_m}{M}\right)^{1/3} \left(\frac{3J_2}{k_2}\right)^{2/3} < \frac{M_m}{M} < \left(\frac{J_{22}}{J_2}\right)^{(\text{present})}. \quad (27)$$

Together with formulae (4) and (6 - 7), this double inequality enables us to constrain the values of  $\mu$ ,  $k_2$ , and

$r/R$  at the time of synchronisation, and then to write down a slightly more accurate constraint on  $M_m/M$  itself. Derived in Appendix B, these constraints read:

$$1.17 < k_2 < 1.44 , \quad (28)$$

$$1.44 \text{ GPa} > \mu > 0.20 \text{ GPa} , \quad (29)$$

$$5.91 < \frac{r}{R} < 6.26 . \quad (30)$$

The right-hand bounds of these inequalities are dictated by geophysical considerations provided in Section 1.3, equations (5), (6), and (8). Given the low value of  $\mu$ , these bounds relate to a situation where the moon synchronised Mars at an early time (perhaps, before the end of the magma ocean stage).

The left-hand bounds in the above inequalities stem from the synchronous-state stability condition, equation (21). Incorporating, specifically, the higher value of  $\mu$  in equation (29), these limits correspond to a scenario where the moon synchronised Mars at the beginning of solidification when the crust was already present or forming. This timing, however, is hypothetical, and its confirmation requires detailed modelling.

The resulting constraint on Nerio's mass is:

$$3.23 \times 10^{-2} \gtrsim 3.225 \times 10^{-2} \gtrsim \frac{M_m}{M} \gtrsim 2.81 \times 10^{-2} . \quad (31)$$

Here, like in inequalities (28 - 30), the right-hand bound  $2.81 \times 10^{-2}$  corresponds (via equation 22) to the maximal value of  $k_2$  and (through equations 5 and 6) to the minimal  $\mu$ . The left-hand bound  $3.225 \times 10^{-2}$  corresponds in a similar way to the minimal value of  $k_2$  and the maximal  $\mu$ . We have deliberately abstained from rounding it, in order to keep it separate from an almost identical bound  $3.23 \times 10^{-2}$  originating from very different considerations, equation (26). With rounding, the two upper-bound values coincide, despite their different provenance.

## 5 Did Nerio reach the marginal point? Did it reach the Roche limit?

In agreement with equation (31), we set the mass of Nerio to be

$$M_m = 0.03 M = 1.89 \times 10^{22} \text{ kg} .$$

The semimajor axis  $a_3$  at the marginal point 3 in Figure 2 is the radius  $r$  of the synchronous orbit at that point, and is given by formula (20). For  $M_m = 0.03 M$ , it is

$$a_3 = 2.0629 \times 10^7 \text{ m} . \quad (32)$$

Its insertion into expression (17) gives us the rotation rate of Mars at that moment of time:

$$\Omega_3 = 7.0294 \times 10^{-5} \text{ rad s}^{-1} . \quad (33)$$

The current rate of Mars' rotation is

$$\Omega^{(\text{present})} = 7.088 \times 10^{-5} \text{ rad s}^{-1} , \quad (34)$$

only a tiny bit faster than  $\Omega_3$ . Given the uncertainties in Nerio's mass and in Mars' radius prior to the LHB, the fourth, third, and possibly even the second decimal places in the values of  $a_3$  and  $\Omega_3$  should be interpreted with caution, see Appendix E.1. So, *to the precision available*, we obtain:

$$\Omega^{(\text{present})} \simeq \Omega_3 . \quad (35)$$

This coincidence is so exact as to be somewhat fortuitous, but not displeasing. It would be too risky to conclude from it that the moon disintegrated exactly at the marginal point, and that Mars' rotation rate has survived unchanged since that event. Assuming that Mars' differentiation had long been completed by that time, and recalling that since then the solar tides have been slowing down Mars' spin, we deduce that Mars' rotation rate at the instant of Nerio's destruction should have been slightly higher than  $\Omega_3$  — to be later slowed down by solar tides back to  $\Omega^{(\text{present})} \simeq \Omega_3$ . This means that Nerio had transcended the marginal point and started moving up the tangent track in Figure 2, reducing its separation from Mars and spinning Mars up.

As will be explained below, Nerio's creep from point 2 to point 3 in Figure 2 was slow before the emergence of the palaeo ocean (i.e., while Mars'  $|K_2| = k_2/Q$  was small), but accelerated greatly after the ocean's emergence, because  $|K_2|$  increased by an order or two of magnitude. Therefore, Nerio reached the marginal point right after the ocean formation — i.e., shortly after the beginning of LHB.<sup>5</sup>

Nerio's destruction during the LHB did not necessarily take place right at the marginal point, but could as well have happened slightly later. This would give Nerio some time to crawl a bit up the tangent track in Figure 2, and to accelerate Mars' rotation slightly above its present value.

Now, could Nerio have somehow survived the LHB and migrated all the way inward to the Roche limit, disintegrating only there? Had it done so, it would have endowed Mars with a faster rotation rate than today. For solar tides to subsequently slow down Mars' spin back to the present value  $\Omega^{(\text{present})} \simeq \Omega_3$ , the early Martian

<sup>5</sup> A large amount of water was delivered to Mars by the comets and water-rich carbonaceous asteroids arriving in abundance during the LHB. This is why the birth of the Martian ocean coincided with the beginning of the LHB.

palaeo-ocean would then have needed to be much more dissipative and/or to have persisted far longer than current models suggest. This scenario therefore appears unlikely, based on our present understanding.

To discuss these issues quantitatively, we need to know how Mars' rotation rate evolved as a synchronous Nerio migrated from point 2 toward the marginal point 3, and how it evolved later, after Nerio was released from synchronism at point 3 and began travelling inward along the tangent straight track in Figure 2.

## 6 Evolution of Mars' rotation before Nerio's demise

A calculation in Section 3 explains that the synchronisation took place, in Figure 1, on a dynamical track 1 residing above track 2 tangent to the cubical curve. To understand how high track 1 was positioned above track 2, we first recall that the action of solar tides is an adiabatic process, in that a dynamical track (straight line 1 in Figure 1) is very slowly evolving leftwards (or downwards), approaching the tangent straight line 2 and staying parallel to it. Owing to this slowness, the evolving synchronous state (the right-hand crossing point of the slowly moving straight line and the cubical curve in Figure 1) reaches the marginal point when the Martian crust is already formed.

In Figure 2, this evolution is depicted by a slow motion of point 2 to the marginal point 3.

### 6.1 General formalism: the action of solar tides on a planet with a synchronous moon

We begin by deriving a general analytic expression for the tidal evolution of a planet's spin under the influence of tides raised by its host star, in systems where the planet's rotation has been synchronised by its moon. To our knowledge, such an expression has never appeared in the literature heretofore.

The planet's angular acceleration is produced by the two counter-directed actions from the tidal torques generated by the star and the moon:

$$\dot{\Omega} = \dot{\Omega}|_{\text{solar}} + \dot{\Omega}|_{\text{“lunar”}}, \quad (36)$$

where, for brevity, the moon's action is frivolously termed as “lunar”, in analogy with the Earth's case.

The semidiurnal part of the solar torque acting on Mars is given by the third line of equation (116) in

Efroimsky (2012):

$$\begin{aligned} \mathcal{T}|_{\text{solar}} &= \frac{3}{2} M_{\odot} \frac{GM_{\odot}}{a_M^3} \left(\frac{R}{a_M}\right)^3 R^2 K_2(\omega) \\ &= -\frac{3}{2} M_{\odot} \frac{GM_{\odot}}{a_M^3} \left(\frac{R}{a_M}\right)^3 R^2 \mathcal{I}m\{\bar{k}_2(\omega)\} \end{aligned} \quad (37)$$

with  $M_{\odot}$  being the solar mass, and  $M$ ,  $R$ ,  $K_2(\omega)$ , and  $\bar{k}_2(\omega)$  representing the Martian mass, radius, quality function, and complex Love number.<sup>6</sup> The notation  $\omega$  stands for the semidiurnal tidal Fourier mode of the solar tides exerted on Mars:  $\omega \equiv \omega_{2200} = 2(n_M - \Omega)$ , where  $n_M$  is the mean motion of Mars about the Sun, while  $\Omega$  is Mars' rotation rate (coinciding with Nerio's mean motion  $n$ ). Since  $n_M \ll \Omega$ , we can write  $\omega \approx -2\Omega$ , and therefore,

$$K_2(\omega) \approx -K_2(2\Omega) = -\frac{k_2(2\Omega)}{Q(2\Omega)}. \quad (38)$$

This yields:

$$\dot{\Omega}|_{\text{solar}} = \frac{\mathcal{T}|_{\text{solar}}}{\xi MR^2} = -\frac{3}{2\xi} \frac{M_{\odot}}{M} \frac{GM_{\odot}}{a_M^3} \left(\frac{R}{a_M}\right)^3 K_2(2\Omega). \quad (39)$$

The synchronous Nerio is acting on Mars with a torque which, according to equation (14), contributes the following input into Mars' angular acceleration:

$$\dot{\Omega}|_{\text{“lunar”}} = -\frac{1}{2} X a^{-1/2} \dot{a}. \quad (40)$$

This input is positive, because  $\dot{a}$  is negative when Nerio is approaching Mars. This inward evolution is taking place when the system, while remaining synchronous, is slowly moving from point 2 to point 3 along the hyperbola in Figure 2. The slowly evolving synchronism implies that the separation between Mars and Nerio is always equal to the evolving synchronous radius  $r$  given by equation (10):

$$a = r = \left(\frac{G(M + M_m)}{\Omega^2}\right)^{1/3}, \quad (41)$$

for which reason

$$\dot{\Omega} = -\frac{3}{2} \sqrt{G(M + M_m)} a^{-5/2} \dot{a}. \quad (42)$$

Together, equations (36), (39), (40), and (42) produce:

$$\begin{aligned} \frac{1}{2} \left(X - 3 \sqrt{G(M + M_m)} a^{-2}\right) a^{-1/2} \dot{a} = \\ -\frac{3}{2\xi} \frac{M_{\odot}}{M} \frac{GM_{\odot}}{a_M^3} \left(\frac{R}{a_M}\right)^3 K_2(2\Omega), \end{aligned} \quad (43)$$

<sup>6</sup> We abide by the convention  $K_2 \equiv -\mathcal{I}m\{\bar{k}_2\}$ , with a “minus” sign, in order to ensure that the negative argument of the complex number  $\bar{k}_2$  represents a phase lag, not advance.

an expression applicable to any system comprising a host star, a planet, and a moon orbiting synchronously with the planet's rotation.

We now employ this expression to estimate the duration of Nerio's stay in the transient synchronism with Mars.

## 6.2 For how long did Nerio stay in the transient synchronism before reaching the marginal point?

Owing to the solar tides in Mars, Nerio's synchronous state is transient. In Figure 2, point 2 is slowly moving to the marginal point 3 from which Nerio will begin its descent towards the Roche limit. Our goal is to estimate the duration  $t_3 - t_2$  of this creep from point 2 to point 3.

### 6.2.1 Before the ocean formation

After a short magma-ocean stage, the Martian mantle became a Maxwell material with shear rigidity  $\mu$  and shear viscosity  $\eta$ . As demonstrated in Appendix C, equation (85), the planet's quality function acquired the form <sup>7</sup>

$$K_2(2\Omega) = \frac{D}{\Omega}, \quad (44)$$

where

$$D = \frac{3}{4} \left( \frac{\mathcal{B}_2 \mu}{1 + \mathcal{B}_2 \mu} \right)^2 \frac{1}{\mathcal{B}_2 \eta}. \quad (45)$$

With equation (41) taken into account, expression (44) becomes

$$K_2(2\Omega) = D \frac{a^{3/2}}{\sqrt{G(M + M_m)}}. \quad (46)$$

The insertion of this expression into formula (43) yields the following differential equation of spin-orbital evolution of a synchronised planet-moon system:

$$\left( \frac{M_m}{R^2} a^{-2} - 3\xi(M + M_m)a^{-4} \right) da = -3D \frac{M_\odot^2 R^3}{M a_M^6} dt. \quad (47)$$

<sup>7</sup> Owing to the extreme shortness of the magma-ocean stage, all or most of the evolution from point 2 to point 3 in Figure 2 was taking place when the mantle was already Maxwell, not liquid, and the viscosity was high enough to ensure that the forcing frequency was located to the right of the peak in Figure 4. This ensures that the quality function assumed the form given by equation (44). As explained in Appendix C, equation (83), these conditions are satisfied for  $|\omega| > |\omega_{\text{peak}2}| = \tau_M^{-1}/(1 + \mu\mathcal{B}_2) \approx \tau_M^{-1} = \mu/\eta$ , i.e., for

$$\tau_M > |\omega|^{-1} = (2\Omega)^{-1} \approx 0.83 \times 10^4 \text{ s},$$

where the estimate  $\Omega \approx 0.6 \times 10^{-4}$  rad/s is borrowed from Figure 2.

Integrating thereof renders the time of Nerio's stay in synchronism:

$$t_3 - t_2 = \frac{1}{3D} \left[ \frac{M_m M}{M_\odot^2} \frac{a_m}{a_3} \left( \frac{a_m}{R} \right)^5 \left( 1 - \frac{a_3}{a_2} \right) - \xi \left( 1 + \frac{M_m}{M} \right) \left( \frac{M}{M_\odot} \right)^2 \left( \frac{a_m}{R} \right)^3 \left( \frac{a_m}{a_3} \right)^3 \left( 1 - \left( \frac{a_3}{a_2} \right)^3 \right) \right], \quad (48)$$

where 2 and 3 are the starting and finishing points in Figure 2.

Using the value of  $a_3$  given by expression (32), and borrowing the other parameters' values from Table 1, we arrive at

$$t_3 - t_2 = \frac{1}{D} \left[ 1.4268 \times 10^{13} \left( 1 - \frac{a_3}{a_2} \right) - 0.4752 \times 10^{13} \left( 1 - \left( \frac{a_3}{a_2} \right)^3 \right) \right]. \quad (49)$$

This interval of time is evidently sensitive to the altitude change  $a_2 - a_3$  experienced by the moon between its synchronisation and the departure from the synchronous orbit at point 3.

To obtain a crude estimate for  $t_3 - t_2$ , we choose a realistic value  $|K_2| \approx 0.7 \times 10^{-2}$ , to which the following value of  $D$  corresponds:

$$D = 0.52 \times 10^{-6} \text{ s}^{-1}. \quad (50)$$

For an  $a_2 - a_3 = 10,000$  km descent, we then obtain a prohibitively long value of  $t_3 - t_2 = 8.3$  Gyr exceeding the solar system age. In a less extreme case of a  $a_2 - a_3 = 1000$  km, Nerio's stay in the evolving transient synchronism lasts for  $t_3 - t_2 = 2.1$  Gyr, which is still too long. Indeed, given the current absence of any significant latitudinal distribution in the early Martian cratering record, Nerio's demise should be assigned to the æons predating the termination of the LHB, that is, to a time earlier than  $\approx 3.8$  Gyr ago. For the altitude change  $a_2 - a_3$  of several thousand km, this would require the value  $K_2 \approx 0.7 \times 10^{-1}$  too high for an oceanless planet. We conclude that for realistic values of the parameters, Nerio was unable to reach the marginal point 3 in Figure 2 before the formation of a palaeo ocean on Mars.

Had Nerio been eliminated by a collision somewhere between points 2 and 3, Mars' rotation rate  $\Omega$  corresponding to that moment of time would be lower than  $\Omega^{(\text{present})} \approx \Omega_3$ , which is impossible, given that the subsequent action by solar tides has been working since then to further decelerate Mars' rotation. Therefore, Nerio did reach the marginal point — which indicates that Nerio's lifespan overlapped with that of the palaeo ocean on Mars, as will become clear shortly.

### 6.2.2 After the ocean formation

The system's evolution described by the above equations (47 - 49) accelerated after Mars developed a palaeo ocean. Depending on its shape and depth, the ocean boosted the value of Mars'  $K_2$  by at least an order or two of magnitude, and thereby evicted Nerio by shortening the time of its stay in the synchronous orbit. For a planet with an ocean, the estimate  $K_2 \simeq 0.2$  is very conservative, see Appendix D for details. Through equation (44), this value of  $K_2$  corresponds to  $D = 1.5 \times 10^{-5} \text{ s}^{-1}$ , whose substitution into expression (49) reduces the value of  $t_3 - t_2$  by an order of magnitude.<sup>8</sup> Thus, even for a  $a_2 - a_3 = 10,000 \text{ km}$  descent, the resulting time  $t_3 - t_2$  is only 0.29 Gyr, which means that Nerio reached point 3 shortly after the onset of the LHB, but well before its completion. For a shorter fall of  $a_2 - a_3 = 1000 \text{ km}$ , the required duration of Nerio's synchronous creep becomes as short as  $t_3 - t_2 = 0.073 \text{ Gyr}$ .

### 6.2.3 Conclusions to Section 6.2

Nerio was initially crawling very slowly from its synchronisation point 2 towards the marginal point 3 in Figure 2, and failed to reach it by the start of the LHB, some 4.1 Gyr ago. Having stayed for that long in synchronism with Mars, Nerio ensures that Mars' tidal bulge froze, and the triaxial form of the planet stayed thereafter.

As soon as the LHB brought enough water for the ocean to emerge, Nerio quickly arrived at point 3, and departed therefrom onto the track leading to the Roche limit, the straight line in Figure 2, which is tangent to the cubical curve at point 3. Shortly after the departure, Nerio was eliminated by the LHB. Mars was left with the angular velocity  $\Omega$  corresponding to the moment of Nerio's demise. Mars' rotation rate was then slowly reduced by solar tides.

To summarise, Nerio's stay in synchronism prior to Mars' ocean formation was sufficiently long for the Nerio-produced tidal bulge on Mars to get frozen. On the other hand, Nerio's crawl towards the marginal point accelerated abruptly following the ocean formation at the start of the LHB, leading to near-immediate arrival at point 3 where Nerio got unsynchronised and began its

<sup>8</sup> For a planet with an ocean,  $K_2$  is not necessarily inversely proportional to  $\Omega$  as in equation (44). The actual frequency dependence is more complex and contains sharp peaks corresponding to tides' resonances with the normal modes of the ocean's basin (Auclair-Desrotour et al., 2023; Farhat et al., 2022). Therefore our estimates, like 0.83 Gyr for a 10,000 km descent, or 0.21 Gyr for a 1000 km descent should not be taken too literally. Our goal was simply to illustrate that the emergence of an ocean greatly accelerates the process. For a crude estimate intended for a short time interval, the average shape of the frequency-dependence of  $K_2$  is unimportant, of relevance being only the order of magnitude of  $K_2$ . Finally, the presence of peaks in the frequency dependence only adds to dissipation and shortens the resulting interval  $t_3 - t_2$ .

descent. This descent was then quickly interrupted, because the moon was likely to get destroyed by the LHB before reaching the Roche radius.

## 7 Evolution of Mars' rotation after the moon's demise

After Nerio disintegrates, Mars becomes subject to solar tides only, its angular velocity  $\Omega$  being gradually decelerated by them.

### 7.1 Despinning of an oceanless Mars

As we saw in Section 5, Mars' rotation rate at the moment of Nerio's demise coincided or virtually coincided with the current rotation rate.

Mars' secular despinning rate is

$$\dot{\Omega} = \frac{1}{\xi MR^2} \mathcal{T} \Big|_{\text{solar}} \propto \frac{1}{\xi MR^2} \mathcal{T}_{22} \Big|_{\text{solar}}, \quad (51)$$

where  $\mathcal{T}_{22}$  is the semidiurnal component of the solar tidal torque  $\mathcal{T}$ , and is given by expression (37).

Mars is now cold, its quality function assuming as low a value as  $K_2 \equiv k_2/Q = 0.174/93.0 = 1.87 \times 10^{-3}$  (Konopliv et al., 2020; Pou et al., 2022). Inserting it into the above expression for  $\mathcal{T}_{22}$ , we find that at present this despinning torque is extremely weak. By equation (51), its effect on Mars' spin evolution is only

$$\begin{aligned} \dot{\Omega} \Big|_{\text{solar}}^{(\text{present})} &= -8.801 \times 10^{-25} \text{ rad s}^{-2} \\ &= -1.808 \times 10^{-1} \text{ mas yr}^{-2}. \end{aligned} \quad (52)$$

Superimposed on this secular effect are rotation variations induced by geophysical and atmospheric processes (like the redistribution of carbon dioxide),<sup>9</sup> but at this point we are interested in the secular effect solely.

If we assume that the mean tidal deceleration rate over the past æons has been the same as today, equation (52), and if we also accept that Nerio was gone some 4 Gyr ago, this will leave us with the following estimate for the ensuing change in the angular velocity:

$$\Delta\Omega^{(\text{body tide})} = -\dot{\Omega} \Big|_{\text{solar}}^{(\text{present})} \times 4 \text{ Gyr} = -1.11 \times 10^{-7} \text{ rad/s}, \quad (53)$$

which is almost three orders of magnitude less than the range of spin rates we are dealing with in Figure 2. We

<sup>9</sup> Basing their analysis on *InSight* radio tracking, Le Maistre et al. (2023) concluded that Mars' rotation is currently accelerating at the rate of

$$\dot{\Omega} \Big|_{\text{total}}^{(\text{present})} = 19.0 \times 10^{-24} \text{ rad s}^{-2} = 3.9 \text{ mas yr}^{-2},$$

exceeding by a factor of  $\simeq 22$  the solar decelerating input (52). We presume that this acceleration, if confirmed by future missions, is not a secular effect, by distinction from the permanent input (52).

see that for solar tides to despin an oceanless Mars to exactly the present rotation rate value, the timing of Nerio’s demise ought to have been very precise, a fine tuning of sorts.

In reality, the  $K_2$  of the solid Mars was certainly higher in the past than today. Still, even an order of magnitude increase of our estimate (53) would be insufficient to evade fine tuning. The presence of an ocean, however, mends matters.

## 7.2 Despinning due to a shallow ocean

Sufficiently long-lived in geological terms, the ocean should have had significant implications for the planet’s rotational history. Our goal is to estimate how efficient Mars’ despinning by solar tides might have been after Nerio’s destruction. To this end, we write:

$$\begin{aligned} \Delta\Omega &= \int \frac{\mathcal{T}|_{\text{solar}}}{\xi MR^2} dt \\ &\propto \frac{\Delta t}{\xi MR^2} \mathcal{T}|_{\text{solar}} \propto \frac{\Delta t}{\xi MR^2} \mathcal{T}_{22}|_{\text{solar}}, \end{aligned} \quad (54)$$

the torque being given by expression (88).

While the above integral covers the entire interval from Nerio’s demise to the present, the overwhelming contribution to the spin change  $\Delta\Omega$  occurred over the period  $\Delta t$  spanning Nerio’s demise to the ocean’s disappearance.

The main phase of the Martian palaeo-ocean lasted over the Noachian period, 4.1 - 3.7 Byr ago (Clifford and Parker, 2001). Recent studies, however, offer evidence in favour of the ocean remaining stable until the end of the Hesperian period, 3 Byr ago (Schmidt et al., 2022). Thus the ocean existed for about 1.1 Gyr. As we found in Section 6.2.2, Nerio may still have stayed synchronous over a fraction of Gyr. So the time overlap  $\Delta t$  of Nerio’s existence and the ocean’s presence was slightly shorter than 1.1 Gyr. We therefore shall set

$$\Delta t \simeq 1 \text{ Gyr} . \quad (55)$$

Equation (54) should not be taken too literally. It is not simply a crude estimate, but certainly an underestimate. As explained in Appendix D, an ocean basin can sustain a spectrum of eigenfrequencies, one or several of which may resonate with some tidal mode. Therefore the torque may demonstrate sharp and high peaks over the time span  $\Delta t$ . The peaks may be caused by the basin shape’s resonances not only with the semidiurnal mode present in expression (54), but also with other modes (say, one with  $\{lm\}=\{21\}$ ), which are neglected in that expression. These effects will be working to increase

$\Delta\Omega$ . With this caveat in mind, and with  $|K_2| = 0.2$  as explained in Appendix D, equations (54) and (88) produce:

$$\Delta\Omega \gtrsim -\frac{3}{2\xi} \frac{M_\odot}{M} \frac{GM_\odot}{a_M^3} \left(\frac{R}{a_M}\right)^3 |K_2| \Delta t \approx 0.33 \times 10^{-5} \text{ rad s}^{-1} . \quad (56)$$

Consequently, Mars’ angular velocity at the moment of Nerio’s demise was

$$\Omega = \Omega^{(\text{present})} + \Delta\Omega \gtrsim 7.42 \times 10^{-5} \text{ rad s}^{-1} , \quad (57)$$

which is still about equal to, or only very slightly larger than, Mars’ rotation rate  $\Omega_3 \approx 7.03 \times 10^{-5} \text{ rad/s}$  at the marginal point. Therefore, as expected, Nerio was destroyed in the vicinity of the marginal point, well before it could approach the Roche limit.

## 8 Could Nerio have crossed the Roche radius?

Could Nerio have somehow survived the LHB hazards and made it all the way to the Roche limit, disintegrating only there?

As demonstrated in Appendix E.1 (see also Figure 3), Mars’ rotation rate at the time of Nerio’s hypothetical entering the Roche limit was (for  $M_m = 0.03 M$ ) as high as  $\Omega_R = 1.4823 \times 10^{-4} \text{ rad/s}$ . For this rate to be subsequently reduced by solar tides down to  $\Omega^{(\text{present})} = 0.7088 \times 10^{-4} \text{ rad/s}$ , Mars’ quality function would have to be  $K_2 \simeq 4.7$ , see Appendix E.2. Presently available models provide no indication that planets with oceans are so highly dissipative. Unless such indication appears in future models of Mars’ ocean, we should deem this scenario of Nerio’s demise unrealistic.

## 9 Conclusions

We have investigated the orbital stability and demise of the hypothetical moon Nerio, which had endowed Mars with its initial triaxiality.

Owing to the action of solar tides, Nerio’s synchronous state was transient, a generic fact pertinent to all synchronous moons (see, e.g. Makarov and Efroimsky (2025) and references therein). Nerio’s synchronous state was adiabatically evolving towards a marginal orbit (*‘marginal point’*), the one where Nerio’s orbit became unstable. Except for an extremely brief magma-ocean stage, the tidal parameter  $k_2/Q$  of the oceanless Mars assumed low values, wherefore the evolution of Nerio’s orbit towards the marginal orbit was slow. It however became rapid as soon as the LHB delivered enough water for the formation of a palaeo ocean, which boosted the value of Mars’  $k_2/Q$ .

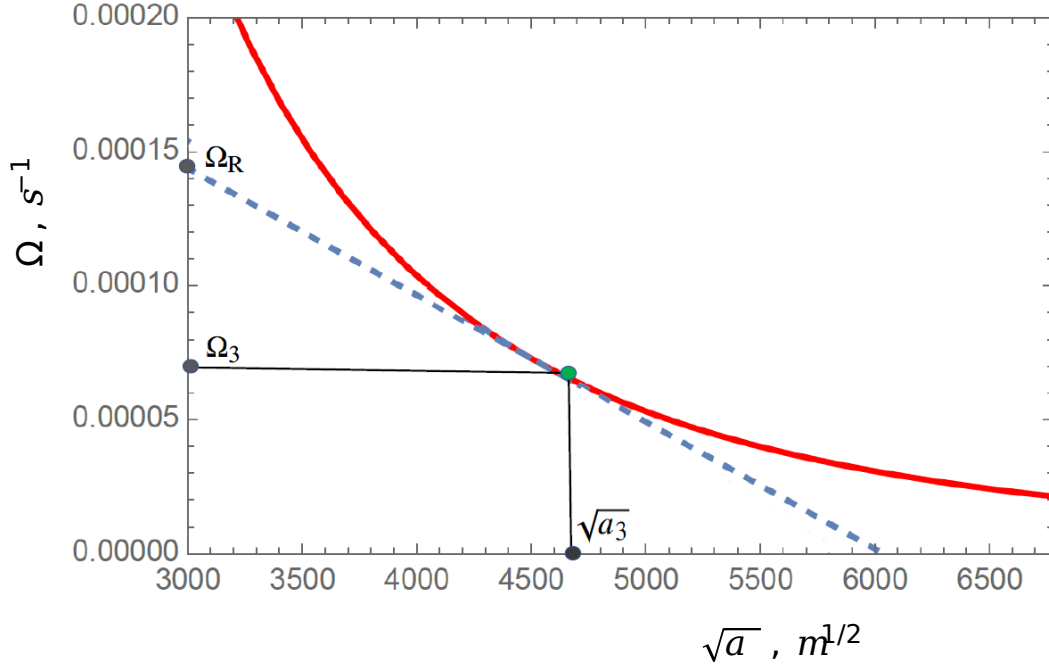


Figure 3 If Nerio survived the LHB and made it all the way to the Roche limit, then, for  $M_m = 0.03M$ , the spin rate of Mars at the time of Nerio’s crossing the Roche radius was  $\Omega_R = 1.4823 \times 10^{-4}$  rad/s, equation (94).

On reaching the marginal orbit, Nerio left synchronism and spiralled down, further accelerating Mars’ spin. Remarkably, Mars’ rotation rate at the desynchronisation moment matches its present-day value to the first decimal place. This coincidence should not be over-interpreted, because the post-desynchronisation evolution comprised Mars’ continued spin-up during Nerio’s fall (until Nerio’s demise amid the LHB) and the subsequent despinning of Mars by solar tides.

A calculation based on a very conservative estimate for  $k_2/Q$  of a Mars with an ocean shows that, after Nerio’s demise, Mars’ despinning by solar tides was a weak effect. This fact indicates that the LHB destroyed Nerio shortly after its orbit reached the marginal point. (We remind that Mars’ rotation rate at that moment virtually coincides with its present-day value.)

Based on our current knowledge of dissipation in ocean-bearing planets, Nerio’s reaching the Roche limit intact is unlikely. To descend all the way to the Roche radius, Nerio would have to accelerate Mars’ rotation to a higher value. To subsequently reduce that value by solar tides, the Mars with an ocean would have to be more dissipative than suggested by the presently available models. Unless future models prove Mars’ ocean to have been much more dissipative, we should regard Nerio’s fall into the Roche limit as unrealistic — though this viewpoint may be reconsidered should new data on Mars’ palaeo ocean show up.

## Acknowledgements

The author extends special thanks to Valeri V. Makarov for valuable advice and numerous stimulating discussions, without which this work would have never been completed. The author is also grateful to Pierre Auclair-Desrotour, Rory Barnes, Mohammad Farhat, Xuan Ji, and Jérémy Leconte for consultations and references.

## Appendix

### A The mass of the young Sun

The combined mass loss to the solar wind and the fusion of hydrogen to helium in the solar core make the young Sun’s mass  $M_\odot$  higher than the present mass  $M_\odot^{(\text{present})}$ . At present, the combined effect of the solar wind and hydrogen-into-helium conversion is negligible,<sup>10</sup> which was not the case of the young Sun. While evolutionary models suggest a broad range of values  $M_\odot = (1.01 - 1.07)M_\odot^{(\text{present})}$ , radio observations of young solar analogues indicate that the total amount of mass lost by the Sun in the early stages of its main-sequence evolution was at most 0.4% (Fichtinger et al., 2017). A safer estimate probably comes from a sugges-

<sup>10</sup> Analysis of the NASA Messenger data establishes a relative change of  $GM_\odot$  of  $(-6.13 \pm 1.47) \times 10^{-14} \text{ year}^{-1}$  (Genova et al., 2018).

tion to resolve the Faint Young Sun Paradox by considering a more luminous early Sun than stellar evolution simulations indicate. To that end, the Sun should be endowed at its origin with approximately 5% more mass than it has now (Nandy et al., 2021):

$$M_{\odot} = 1.05 \times M_{\odot}^{(\text{present})} = 2.09 \times 10^{30} \text{ kg} . \quad (58)$$

## B Derivation of formulae (28 - 31)

### B.1 First iteration

A magma-ocean stage, through which Mars underwent within 10 – 20 million years post-accretion (Bouvier et al., 2018), ensured rapid early differentiation. Hence a motivation to endow the MOI factor  $\xi$  with its present-day value  $\xi^{(\text{present})} = 0.36379$ . Using the other values from Table 1, and setting  $(1 + M_m/M)^{1/3} \approx 1$  in inequality (27), we approximate that equality with

$$1.0914 \left( \frac{3J_2}{k_2} \right)^{2/3} < \frac{M_m}{M} < \left( \frac{J_{22}}{J_2} \right)^{(\text{present})} . \quad (59)$$

For values from Table 1, this becomes

$$3.5514 \times 10^{-2} k_2^{-2/3} < \frac{M_m}{M} < 3.2253 \times 10^{-2} . \quad (60)$$

Hence the limitation on the Love number value:  $k_2 > 1.155$ . Rounding this, we arrive at the following constraints:

$$1.16 \lesssim k_2 \lesssim 1.44 , \quad (61)$$

$$1.54 \text{ GPa} \gtrsim \mu \gtrsim 0.20 \text{ GPa} , \quad (62)$$

$$5.84 \lesssim \frac{r}{R} \lesssim 6.26 . \quad (63)$$

The left bound in inequality (61) ensues from formula (60). The left bound in inequality (62) was obtained from equations (61), (6) and (7). The left bound in inequality (63) was then deduced by combining equations (61) and (4b), with  $(1 + M_m/M)^{1/3} \approx 1$  set in the latter.

The right-hand bounds in these inequalities originate from geophysical considerations provided in Section 1.3, e.g. equations (5), (6), and (8). Given the low value of  $\mu$ , these bounds correspond to a situation where the moon synchronised Mars already at the magma ocean stage.

We would reiterate that the left-hand bounds stem from the spin-orbit state stability condition, equation (21). Given the higher value of  $\mu$ , these bounds correspond, arguably, to synchronisation at the beginning of solidification.

Inserting into expression (60) the largest value of  $k_2$  suggested by geophysical reasoning,  $k_2 = 1.44$ , we obtain, after rounding:

$$2.78 \times 10^{-2} \lesssim \frac{M_m}{M} \lesssim 3.23 \times 10^{-2} , \quad (64)$$

the left and right bounds having the same meaning as those in equations (61 - 63).

### B.2 Second iteration

The double inequality (64) demonstrates that  $M_m/M$  is close to  $3 \times 10^{-2}$ , and therefore  $(1 + M_m/M)^{1/3} \approx 1.0099$ . Insertion thereof into expression (4a) renders us, instead of approximation (4b), a more accurate expression

$$\frac{r}{R} = 5.60 \sqrt[3]{k_2} . \quad (65)$$

Insertion of  $(1 + M_m/M)^{1/3} \approx 1.0099$  into inequality (22) gives us

$$1.1022 \left( \frac{3J_2}{k_2} \right)^{2/3} < \frac{M_m}{M} , \quad (66)$$

whence  $k_2 > 1.1726$ . Repeating the entire process from the preceding subsection, we arrive at more accurate constraints:

$$1.17 < k_2 < 1.44 , \quad (67)$$

$$1.44 \text{ GPa} > \mu > 0.20 \text{ GPa} , \quad (68)$$

$$5.91 < \frac{r}{R} < 6.26 . \quad (69)$$

$$2.81 \times 10^{-2} \lesssim \frac{M_m}{M} \lesssim 3.23 \times 10^{-2} , \quad (70)$$

Here the right-hand bounds remained unaltered, as compared to equations (61 - 64), because these bounds come from geophysical reasoning explained in Section 1.3. The left-hand bounds have changed, because they follow from inequality (22), which in the second iteration is taken into account with a higher accuracy.

## C Tides in Mars before the ocean formation

We model the young Mars' tidal response with that of a homogeneous sphere having a complex compliance

$$\bar{J}(\chi) = \text{Re}[\bar{J}(\chi)] + i \text{Im}[\bar{J}(\chi)] . \quad (71)$$

For a Maxwell body, the complex compliance is especially simple:

$${}^{(\text{Maxwell})}\bar{J}(\chi) = J + i \left( -\frac{1}{\eta\chi} \right) = J \left( 1 - \frac{1}{\tau_M \chi} \right), \quad (72)$$

$\eta$  being the shear viscosity,  $J$  being the unrelaxed shear compliance (the inverse of the unrelaxed shear rigidity  $\mu$ ), and  $\tau_M = \eta J = \eta/\mu$  being the Maxwell time.

In these formulae,  $\chi$  is a short notation for the physical frequency exerted in the body by tides. Such frequencies are equal to the absolute values of the corresponding Fourier tidal modes. Using  $\omega$  as a concise notation for a tidal mode,

$$\omega \equiv \omega_{lmpq}, \quad (73)$$

we write the corresponding frequency as

$$\chi \equiv |\omega| = |\omega_{lmpq}|. \quad (74)$$

A degree- $l$  quality function of a tidally perturbed body is defined as

$$K_l(\omega) \equiv k_l(\omega) \sin \epsilon_l(\omega) = \frac{k_l(\omega)}{Q_l(\omega)} \text{Sign } \omega, \quad (75)$$

where  $k_l(\omega)$ ,  $\epsilon_l(\omega)$ ,  $Q_l(\omega)$  are the degree- $l$  Love number, phase lag, and tidal quality factor.

For a homogeneous near-spherical body of rheology  $\bar{J}(\chi)$ , the quality function reads (see, e.g. Efroimsky 2015, Eqn 40):

$$K_l(\omega) \equiv k_l(\omega) \sin \epsilon_l(\omega) = k_l(\chi) \sin \epsilon_l(\chi) \text{Sign } \omega = \quad (76)$$

$$-\frac{3}{2(l-1)} \frac{\mathcal{B}_l \text{Im}[\bar{J}(\omega)] \text{Sign } \omega}{\left( \text{Re}[\bar{J}(\omega)] + \mathcal{B}_l \right)^2 + \left( \text{Im}[\bar{J}(\omega)] \right)^2},$$

where

$$\mathcal{B}_l \equiv \frac{(2l^2 + 4l + 3)}{lg\rho R} = \frac{3(2l^2 + 4l + 3)}{4l\pi G\rho^2 R^2}, \quad (77)$$

$G$  being Newton's gravity constant, and  $g, \rho, R$  being the surface gravity, density, and radius of the body. Below we shall also need a convenient quantity  $\mathcal{A}_l$  often used in the literature:

$$\mathcal{A}_l \equiv \mathcal{B}_l J^{-1} = \mathcal{B}_l \mu. \quad (78)$$

For simple rheologies, like Maxwell or Andrade, the quality function has the form of a kink with one negative and one positive peak, as in Figure 4. For a Maxwell body, equation (72), the quality functions are especially simple:

$$K_l(\omega) = \frac{3}{2(l-1)} \frac{\tau_M \omega \mathcal{A}_l}{1 + (\tau_M \omega)^2 (1 + \mathcal{A}_l)^2}. \quad (79)$$

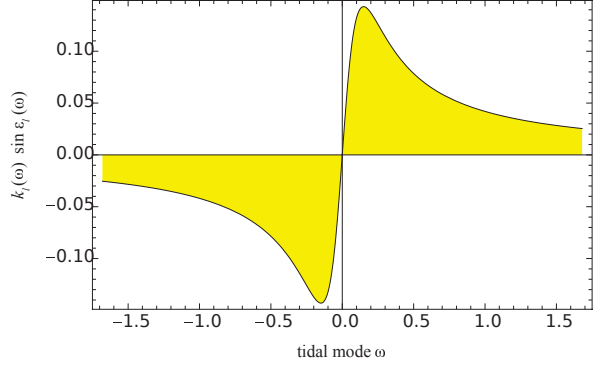


Figure 4 . A typical shape of the quality function  $k_l(\omega) \sin \epsilon_l(\omega)$ , where  $\omega$  is a shortened notation for the tidal Fourier mode  $\omega_{lmpq}$ . (From Noyelles et al. 2014.)

[Mind a misprint in Makarov and Efroimsky (2023, Eqn B.7).]

As demonstrated, e.g. in Walterová et al. (2023, Section 4.4), the peak of this kink is located at

$$\omega_{\text{peak}_l} = \pm \frac{\tau_M^{-1}}{1 + \mathcal{A}_l}, \quad (80)$$

and has a viscosity-independent magnitude

$$K_l^{(\text{peak})} = \pm \frac{3}{4(l-1)} \frac{\mathcal{A}_l}{1 + \mathcal{A}_l}. \quad (81)$$

[Mind a misprint in Bagheri et al. (2021, Eqn 62).]

The magnitude remains independent of viscosity also when the mantle cools down and begins to obey the Andrade rheology, which is caused by the emergence of transient processes. These dissipation mechanisms usually show up at frequencies much higher than the peak frequency (80), see Walterová et al. (2023).

From equation (79), we deduce that for a Maxwell body a quality function  $K_l(\omega)$  is nearly linear in the interval between peaks:<sup>11</sup>

$$|\omega| < |\omega_{\text{peak}_l}| \implies \quad (82)$$

$$K_l(\omega) \simeq \frac{3}{2(l-1)} \tau_M \omega \mathcal{A}_l = \frac{3}{2(l-1)} \frac{\mathcal{A}_l}{1 + \mathcal{A}_l} \frac{\omega}{|\omega_{\text{peak}_l}|}.$$

Outside the peaks, the function is falling off as the inverse  $\omega$ :

$$|\omega| > |\omega_{\text{peak}_l}| \implies \quad (83)$$

$$K_l(\omega) \simeq \frac{3}{2(l-1)} \frac{\mathcal{A}_l (\tau_M \omega)^{-1}}{(1 + \mathcal{A}_l)^2} = \frac{3}{2(l-1)} \frac{\mathcal{A}_l}{1 + \mathcal{A}_l} \frac{|\omega_{\text{peak}_l}|}{\omega}.$$

<sup>11</sup> In the product  $\tau_M \omega \mathcal{A}_l = \mathcal{B}_l \eta \omega$ , the dependence on  $\mu$  cancels, and the resulting quality function in equation (82) depends on the product of viscosity and frequency:  $K_2(\omega) = \frac{3}{2(l-1)} \mathcal{B}_l \eta \omega$ .

As explained in Section 6.1, in the setting of our concern  $\omega$  is the semidiurnal frequency of the solar tides on Mars, and is equal, to a good precision, to  $-2\Omega$ , where  $\Omega$  is Mars' rotation rate. Consequently, a quality function  $K_l(\omega)$  becomes  $-K_l(2\Omega)$ .

We now need to know if the the tidal frequency  $2\Omega$  is located between the peaks in Figure 4 or outside the inter-peak interval. To this end, we recall that  $\Omega$  is related to the semimajor axis  $a$  by equation (17), where the semimajor axis is identified with the synchronous radius:  $a = r$ . Equation (30) sets the maximal value of the synchronous radius:  $r < 6.26R$ . Therefore,

$$\begin{aligned} 2\Omega &= 2\sqrt{\frac{G(M+M_m)}{r^3}} \\ &> 2\sqrt{\frac{G(M+M_m)}{R^3}} 6.26^{-3/2} = 1.36 \times 10^{-4} \text{ s}^{-1}, \end{aligned} \quad (84)$$

a value to be compared with the positive peak frequency rendered by expression (80).

During the magma-ocean stage,  $\mu$  was at its minimum, so  $1 + \mathcal{A}_l \approx 1$ , and the positive peak frequency was close to the inverse Maxwell time:  $\omega_{\text{peak}} \approx \tau_m^{-1} = \mu/\eta$ . Whether  $\tau_m^{-1}$  was higher or lower than  $10^{-4} \text{ s}^{-1}$  at the magna-ocean stage is model-dependent. It is therefore unclear whether the tidal response of the planet during that stage should be described by equation (82) or (83). On the other hand, the duration of that stage was shorter than 20 million years (Bouvier et al., 2018), so the degree of system evolution over that period may be neglected as compared with the subsequent changes of  $\Omega$  and  $r$ .

After the onset of crystallisation, the mantle viscosity could have resided, depending on the moisture content, between  $10^{19}$  and  $10^{21}$  Pa s, at a reference temperature of 1600 K (Breuer and Spohn, 2006). For a shear rigidity of  $\mu \simeq 0.2 \times 10^9$  Pa, the peak frequency was as low as  $\simeq 10^{-11} - 10^{-9} \text{ s}^{-1}$ . Even for a rigidity lower by four orders of magnitude, the peak frequency would still be lower than the semidiurnal frequency given by equation (84).

We thus conclude that over Mars' early evolution, except for a very brief magma-ocean period, the frequency  $2\Omega$  was residing outside the inter-peak interval in Figure 4. Consequently, with the said caveat about the short magma-ocean stage kept in mind, the planet's tidal response was described by expression (83). The quadrupole quality function was

$$K_2(\omega) = \frac{3}{2} \frac{\mathcal{A}_2}{(1 + \mathcal{A}_2)^2} \frac{1}{\tau_m \omega} = \frac{3}{2} \left( \frac{\mathcal{B}_2 \mu}{1 + \mathcal{B}_2 \mu} \right)^2 \frac{1}{\mathcal{B}_2 \eta \omega}. \quad (85)$$

We reiterate that this expression is valid only for  $|\omega| > |\omega_{\text{peak}}|$ .

According to equation (38),  $K(\omega) \approx -K(2\Omega)$ , where

$$K_2(2\Omega) = \frac{D}{\Omega} \quad \text{and} \quad D = \frac{3}{4} \left( \frac{\mathcal{B}_2 \mu}{1 + \mathcal{B}_2 \mu} \right)^2 \frac{1}{\mathcal{B}_2 \eta}. \quad (86)$$

## D Tides on a Mars with an ocean

For bodily tides, a degree- $l$  component of the decelerating tidal torque scales as  $a_M^{-2(l+1)} \mathcal{I}m\{\bar{k}_l\}$ , where  $a_M$  is the semimajor axis of Mars' orbit about the Sun (Efroimsky, 2012, Eqn 106). As customary,  $\bar{k}_l$  signifies a complex Love number, such that  $\mathcal{I}m\{\bar{k}_l\} = -k_l \sin \epsilon_l$ , where  $k_l$  and  $\epsilon_l$  are the frequency-dependent real Love number and phase lag. As explained by Farhat et al. (2022, Appendix K) and Auclair-Desrotour et al. (2023, Section 2.8), the oceanic tidal torque scales similarly, though contains different, oceanic Love numbers. Thus, bodily and oceanic tides can be pictured as a single process — an overall tidal response of the planet, governed by the total Love numbers<sup>12</sup>

$$\bar{k}_{lm}^{(\text{total})} = \bar{k}_l + \bar{k}_{lm}^{(\text{ocean})}, \quad (87)$$

where the first term is the bodily-tide Love number, while the second term is the oceanic Love number. By distinction from the first term, the second term depends on both the degree  $l$  and order  $m$ . As explained in *Ibids.*, this ensues from the Coriolis force influencing the oceanic tidal response, which is not the case for the bodily tides.

The total semidiurnal solar torque (37) then becomes

$$\begin{aligned} \mathcal{T}_{22}^{(\text{total})} &= \frac{3}{2} M_\odot \frac{GM_\odot}{a_M^3} \left( \frac{R}{a_M} \right)^3 R^2 K_{22}^{(\text{total})}(\omega) \\ &= -\frac{3}{2} M_\odot \frac{GM_\odot}{a_M^3} \left( \frac{R}{a_M} \right)^3 R^2 \mathcal{I}m\{\bar{k}_{22}^{(\text{total})}(\omega)\}. \end{aligned} \quad (88)$$

The overall tidal dissipation budget of Earth is dominated by tides in the ocean. While establishing an exact fluid/solid partition is difficult, it is believed that friction in the solid Earth consumes about 5% (Egbert and Ray, 2001) of the tidal power damped. So the ocean dissipates about 20 times more energy than solid Earth.

For other terrestrial planets, however, the tidal response of the ocean can vary greatly, depending on the form of basin, the range of depth, seafloor topography,

<sup>12</sup> The fact that the tidal torque is proportional to  $a_M^{-2(l+1)} \mathcal{I}m\{\bar{k}_l\}$  may, at times, imply a complicated overall  $a_M$ -dependence. Both the solid-body and oceanic Love numbers depend, in different manners, upon the tidal frequencies  $\omega$  involved. There frequencies, in their turn, depend on the mean motion and therefore on the semimajor axis  $a_M$ . This imposes  $a_M$ -dependencies on both  $\mathcal{I}m\{\bar{k}_l\}$  and  $\mathcal{I}m\{\bar{k}_{lm}^{(\text{ocean})}\}$ . Such dependencies may be especially pronounced for the oceanic Love numbers, owing to the basin mode resonances.

and the planet’s rotation rate. Blackledge et al. (2020) argue that, depending on the continental shapes, the oceanic dissipation could vary by five orders of magnitude.

Two thirds of Earth’s oceanic dissipation occur in narrow straits and shallow seas. By distinction from Earth, the entire ocean on Mars was mainly shallow — which served as a booster of dissipation. On the other hand, the shape of the Martian ocean also played a critical role in tidal dynamics. A nearly circular shape with few straits would result in a lower dissipation rate. In contrast, a non-symmetric basin with a jagged and rugged coastline would have supported a rich spectrum of normal modes defined by its geometry. In such a basin, solar forcing could have excited one or more of these modes into resonance during the ocean’s lifetime, potentially increasing oceanic dissipation by orders of magnitude. Further boost could emerge from straits. The exact shape of the Martian palaeo-ocean still remains a subject of exploration.

As of now, the most accurate numerical treatment of which we are aware is provided in the works by Auclair-Desrotour et al. (2018), Farhat et al. (2022) and Auclair-Desrotour et al. (2023). Specifically, Figure 5 in Auclair-Desrotour et al. (2018) illustrates an attempt at constructing frequency-dependencies of  $|K_2|$  for various models of Earth and TRAPPIST-1f. The models were built for planets with deep oceans. While in the case of the Earth the values of  $|K_2|$  at low frequencies are typically below or close to 0.1, resonant peaks at low frequencies rise close to and even above 10.

The palaeo ocean on Mars was shallow and therefore much more dissipative than the oceans modelled in *Ibids.*, for which reason we may safely adopt for it the estimate

$$K_2 \simeq 0.2 , \quad (89)$$

in understanding that a higher value or the presence of peaks would only strengthen our conclusions. Even this conservative value ensures Nerio’s swift arrival at point 3 in Figure 2, see Section 6.2.2.

## E Did Nerio reach the Roche limit?

On arrival at the marginal point (point 3 in Figure 2), Nerio left synchronism and began to follow the track aimed towards the Roche limit — see the straight line, which is tangent to the cubical curve at point 3. Since by the time of Nerio’s arrival at point 3 the LHB was already going on (see Section 6.2.2), Nerio was likely to perish soon. It would nonetheless be of interest to explore if perhaps it had a chance to make it all way to the Roche radius. As we shall see shortly, this scenario would be conceivable

only for an ocean much more dissipative than proposed by the currently available studies.

### E.1 Mars’ rotation rate at the moment of Nerio’s hypothetical crossing of the Roche limit

For  $M_m = 0.03M$ , the values of Nerio’s semimajor axis and Mars’ rotation rate at the marginal point were derived in Section 5:

$$a_3 = 2.0629 \times 10^7 \text{ m} , \quad \Omega_3 = 7.0294 \times 10^{-5} \text{ rad/s} . \quad (90)$$

The slope given by expression (16) assumes the value of

$$X = 4.4643 \times 10^{-8} \text{ m}^{-1/2} \text{ s}^{-1} , \quad (91)$$

wherefrom the integration constant (15) is

$$C = X \sqrt{a_3} + \Omega_3 = 2.7306 \times 10^{-4} . \quad (92)$$

Approximating Nerio’s density with that of our Moon, we obtain for the Roche radius (Efroimsky, 2024, Section 7.1):

$$r_R = 2.32 R = 7.8184 \times 10^6 \text{ m} . \quad (93)$$

Consequently, by equation (14), the Martian spin rate at the moment of Nerio’s crossing the Roche limit is

$$\Omega_R = -X \sqrt{r_R} + C = 1.4823 \times 10^{-4} \text{ rad s}^{-1} , \quad (94)$$

as illustrated by Figure 3.

Needless to say, the fourth and third decimal points in the above values are unreliable because of the uncertainties in Nerio’s mass and in Mars’ radius prior to the LHB. Figure 5 shows the sensitivity of dynamics  $\Omega_R$  to Nerio’s mass  $M_m$ , the range of this mass being established by the double inequality (31).

The maximal possible value  $M_m = 0.0323 M$  produces, via formulae (20), (17), (16), (15), and (14), correspondingly:  $a_3 = 1.9903 \times 10^7 \text{ m}$ ,  $\Omega_3 = 7.4258 \times 10^{-5} \text{ rad s}^{-1}$ ,  $X = 4.9933 \times 10^{-8} \text{ m}^{-1/2} \text{ s}^{-1}$ ,  $C = 2.9703 \times 10^{-4} \text{ rad s}^{-1}$ , and  $\Omega_R = 1.5741 \times 10^{-4} \text{ rad s}^{-1}$ . In Figure 5, this situation is illustrated by the green tangent track, one with a steeper slope.

Similarly, the yellow track, one with a shallower slope, corresponds to  $M_m = 0.0281 M$ ,  $a_3 = 2.1295 \times 10^7 \text{ m}$ ,  $\Omega_3 = 6.6960 \times 10^{-5} \text{ rad s}^{-1}$ ,  $X = 4.3530 \times 10^{-8} \text{ m}^{-1/2} \text{ s}^{-1}$ ,  $C = 2.6784 \times 10^{-4} \text{ rad s}^{-1}$ , and  $\Omega_R = 1.4612 \times 10^{-4} \text{ rad s}^{-1}$ .

### E.2 Subsequent despinning of Mars by solar tides

The question now becomes if solar tides in the Mars with an ocean were capable of slowing down Mars’s rotation

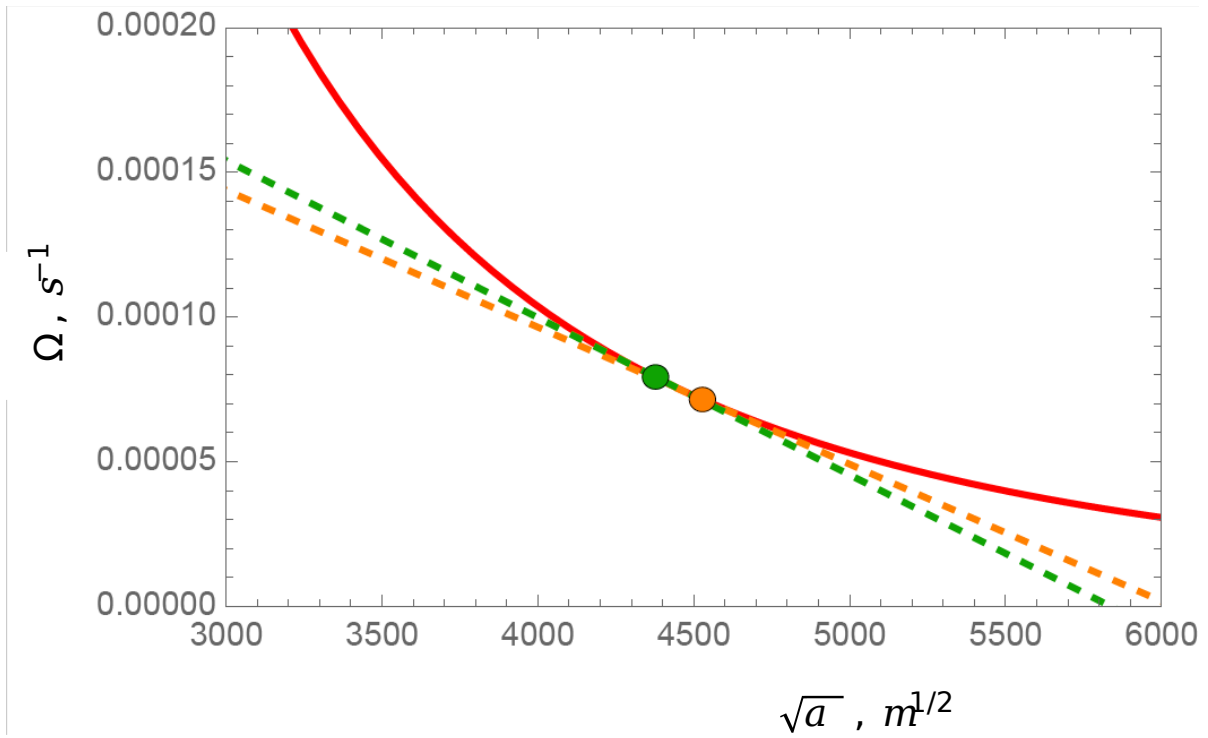


Figure 5 This figure illustrates the sensitivity of  $a_3$ ,  $\Omega_3$ , and  $\Omega_R$  to Nerio's mass  $M_m$ . The green tangent track, one with a steeper slope, corresponds to  $M_m = 0.0323 M$ , and renders  $a_3 = 1.9903 \times 10^7$  m,  $\Omega_3 = 7.4258 \times 10^{-5}$  rad/s, and  $\Omega_R = 1.5741 \times 10^{-4}$  rad/s. The yellow track, one with a shallower slope, corresponds to  $M_m = 0.0281 M$ , and produces  $a_3 = 2.1295 \times 10^7$  m,  $\Omega_3 = 6.6960 \times 10^{-5}$  rad/s, and  $\Omega_R = 1.4612 \times 10^{-4}$  rad/s.

to its present rate. From equation (56), we observe that to overcome the difference  $\Omega_R - \Omega^{(\text{present})} = 0.7735 \times 10^{-4}$  rad/s over a time span of  $\Delta t \approx 1$  Gyr, the ocean-bearing Mars' quality function should have assumed the value

$$K_2 \lesssim \frac{2\xi}{3} \frac{M}{M_\odot} \left(\frac{a_M}{R}\right)^3 \frac{a_M^3}{GM_\odot} \frac{\Delta\Omega}{\Delta t} \approx 4.7, \quad (95)$$

which may be too high in the light of the currently available models of oceans' tidal response.

This precludes us from concluding that Nerio reached the Roche limit, unless future studies indicate that the palaeo ocean on Mars was more dissipative than presumed presently.

## References

- P. Auclair-Desrotour, S. Mathis, J. Laskar, and J. Leconte. Oceanic tides from Earth-like to ocean planets. *Astronomy and Astrophysics*, 615:A23, 2018. doi: 10.1051/0004-6361/201732249.
- Pierre Auclair-Desrotour, Mohammad Farhat, Gwenaél Boué, Mickaël Gastineau, and Jacques Laskar. Can one hear supercontinents in the tides of ocean planets? *Astronomy and Astrophysics*, 680:A13, 2023. doi: 10.1051/0004-6361/202347301.
- Amirhossein Bagheri, Amir Khan, Michael Efroimsky, Mikhail Kruglyakov, and Domenico Giardini. Dynamical evidence for Phobos and Deimos as remnants of a disrupted common progenitor. *Nature Astronomy*, 5:539–543, January 2021. doi: 10.1038/s41550-021-01306-2.
- B. W. Blackledge, J. A. M. Green, R. Barnes, and M. J. Way. Tides on Other Earths: Implications for Exoplanet and Palaeo-Tidal Simulations. *Geophysical Research Letters*, 47(12):e85746, 2020. doi: 10.1029/2019GL085746.
- Laura C. Bouvier, Maria M. Costa, James N. Connelly, Ninna K. Jensen, Daniel Wielandt, Michael Storey, Alexander A. Nemchin, Martin J. Whitehouse, Joshua F. Snape, Jeremy J. Bellucci, Frédéric Moynier, Arnaud Agranier, Bleuenn Gueguen, Maria Schönbachler, and Martin Bizzarro. Evidence for extremely rapid magma ocean crystallization and crust formation on Mars. *Nature*, 558(7711):568–589, June 2018. doi: 10.1038/s41586-018-0222-z.
- Doris Breuer and Tilman Spohn. Viscosity of the martian mantle and its initial temperature: Constraints from crust formation history and the evolution of the magnetic field. *Planetary and Space Science*, 54(2):153–169, 2006. ISSN 0032-0633. doi: <https://doi.org/10.1016/j.pss.2005.08.008>. URL <https://www.sciencedirect.com/science/article/pii/S0032063305000808>.
- Stephen M. Clifford and Timothy J. Parker. The Evolution of the Martian Hydrosphere: Implications for the Fate of a Primordial Ocean and the Current State of the Northern Plains. *Icarus*, 154(1):40–79, 2001. ISSN 0019-1035. doi: <https://doi.org/10.1006/icar.2001.6671>. URL <https://www.sciencedirect.com/science/article/pii/S0019103501006671>.
- Charles C. Counselman, III. Outcomes of Tidal Evolution. *The Astrophysical Journal*, 180:307–316, 1973. doi: 10.1086/151964.
- G. H. Darwin. The Determination of the Secular Effects of Tidal Friction by a Graphical Method. *Proceedings of the Royal Society of London Series I*, 29:168–181, January 1879.
- Michael Efroimsky. Long-Term Evolution of Orbits About A Precessing Oblate Planet: 1. The Case of Uniform Precession. *Celestial Mechanics and Dynamical Astronomy*, 91(1-2):75–108, 2005. doi: 10.1007/s10569-004-2415-z.
- Michael Efroimsky. Bodily tides near spin-orbit resonances. *Celestial Mechanics and Dynamical Astronomy*, 112(3):283–330, 2012. doi: 10.1007/s10569-011-9397-4.
- Michael Efroimsky. Tidal Evolution of Asteroidal Binaries. Ruled by Viscosity. Ignorant of Rigidity. *The Astronomical Journal*, 150(4):98, 2015. doi: 10.1088/0004-6256/150/4/98.
- Michael Efroimsky. A Synchronous Moon as a Possible Cause of Mars' Initial Triaxiality. *Journal of Geophysical Research (Planets)*, 129(10):e2023JE008277, 2024. doi: 10.1029/2023JE008277.
- Gary D. Egbert and Richard D. Ray. Estimates of  $M_2$  tidal energy dissipation from TOPEX/Poseidon altimeter data. *Journal of Geophysical Research*, 106(C10):22,475–22,502, 2001. doi: 10.1029/2000JC000699.
- Mohammad Farhat, Pierre Auclair-Desrotour, Gwenaél Boué, and Jacques Laskar. The resonant tidal evolution of the Earth-Moon distance. *Astronomy and Astrophysics*, 665:L1, 2022. doi: 10.1051/0004-6361/202243445. URL <https://doi.org/10.1051/0004-6361/202243445>.
- Bibiana Fichtinger, Manuel Güdel, Robert L. Mutel, Gregg Hallinan, Eric Gaidos, Stephen L. Skinner, Christene Lynch, and Kenneth G. Gayley. Radio

- emission and mass loss rate limits of four young solar-type stars. *Astronomy and Astrophysics*, 599:A127, 2017. doi: 10.1051/0004-6361/201629886. URL <https://doi.org/10.1051/0004-6361/201629886>.
- Antonio Genova, Erwan Mazarico, Sander Goossens, Frank G. Lemoine, Gregory A. Neumann, David E. Smith, and Maria T. Zuber. Solar system expansion and strong equivalence principle as seen by the NASA MESSENGER mission. *Nature Communications*, 9:289, January 2018. doi: 10.1038/s41467-017-02558-1.
- Peter Goldreich. Inclination of satellite orbits about an oblate precessing planet. *The Astronomical Journal*, 70:5, 1965. doi: 10.1086/109673.
- Pini Gurfil, Valéry Lainey, and Michael Efroimsky. Long-term evolution of orbits about a precessing oblate planet: 3. A semianalytical and a purely numerical approach. *Celestial Mechanics and Dynamical Astronomy*, 99(4):261–292, 2007. doi: 10.1007/s10569-007-9099-0.
- William K. Hartmann, Cathy Quantin, and Nicolas Mangold. Possible long-term decline in impact rates: 2. lunar impact-melt data regarding impact history. *Icarus*, 186(1):11–23, 2007. ISSN 0019-1035. doi: <https://doi.org/10.1016/j.icarus.2006.09.009>. URL <https://www.sciencedirect.com/science/article/pii/S0019103506003150>.
- P. Hut. Tidal evolution in close binary systems. *Astronomy and Astrophysics*, 99:126–140, 1981.
- A. Khan, C. Liebske, A. Rozel, A. Rivoldini, F. Nimmo, J. A. D. Connolly, A. C. Plesa, and D. Giardini. A Geophysical Perspective on the Bulk Composition of Mars. *Journal of Geophysical Research (Planets)*, 123(2):575–611, 2018. doi: 10.1002/2017JE005371.
- Alex S. Konopliv, Sami W. Asmar, William M. Folkner, Özgür Karatekin, Daniel C. Nunes, Suzanne E. Smrekar, Charles F. Yoder, and Maria T. Zuber. Mars high resolution gravity fields from MRO, Mars seasonal gravity, and other dynamical parameters. *Icarus*, 211(1):401–428, January 2011. doi: 10.1016/j.icarus.2010.10.004.
- Alex S. Konopliv, Ryan S. Park, and William M. Folkner. An improved JPL Mars gravity field and orientation from Mars orbiter and lander tracking data. *Icarus*, 274:253–260, 2016. doi: 10.1016/j.icarus.2016.02.052.
- Alex S. Konopliv, Ryan S. Park, Attilio Rivoldini, Rose-Marie Baland, Sebastien Le Maistre, Tim Van Hoolst, Marie Yseboodt, and Veronique Dehant. Detection of the Chandler Wobble of Mars From Orbiting Spacecraft. *Geophysical Research Letters*, 47(21):e90568, 2020. doi: 10.1029/2020GL090568.
- J. Laskar and P. Robutel. The chaotic obliquity of the planets. *Nature*, 361(6413):608–612, February 1993. doi: 10.1038/361608a0.
- S. Le Maistre, A. Rivoldini, A. Caldiero, M. Yseboodt, R.-M. Baland, M. Beuthe, T. Van Hoolst, V. Dehant, W. M. Folkner, D. Buccino, D. Kahan, J.-C. Marty, D. Antonangeli, J. Badro, M. Drilleau, A. Konopliv, M.-J. Pèters, A.-C. Plesa, H. Samuel, N. Tosi, M. Wicczorek, P. Lognonnè, M. Panning, S. Smrekar, and B. W. Banerdt. Spin state and deep interior structure of Mars from InSight radio tracking. *Nature*, 619:733–737, 2023. doi: 10.1038/s41586-023-06150-0.
- Valeri V. Makarov and Michael Efroimsky. Pathways of survival for exomoons and inner exoplanets. *Astronomy and Astrophysics*, 672:A78, April 2023. doi: 10.1051/0004-6361/202245533.
- Valeri V. Makarov and Michael Efroimsky. Initial conditions for tidal synchronisation of a planet by its moon. *Universe*, 11:309, 2025. ISSN 2218-1997. doi: 10.3390/universe11090309. URL <https://www.mdpi.com/2218-1997/11/9/309>.
- Valeri V. Makarov and Alexey Goldin. Chaotic Capture of a Retrograde Moon by Venus and the Reversal of Its Spin. *Universe*, 10(1):15, 2024. doi: 10.3390/universe10010015.
- Dibyendu Nandy, Petrus C. H. Martens, Vladimir Obridko, Soumyaranjan Dash, and Katya Georgieva. Solar evolution and extrema: current state of understanding of long-term solar variability and its planetary impacts. *Progress in Earth and Planetary Science*, 8(1):40, 2021. doi: 10.1186/s40645-021-00430-x.
- L. Pou, F. Nimmo, A. Rivoldini, A. Khan, A. Bagheri, T. Gray, H. Samuel, P. Lognonné, A. C. Plesa, T. Gudkova, and D. Giardini. Tidal Constraints on the Martian Interior. *Journal of Geophysical Research (Planets)*, 127(11):e2022JE007291, 2022. doi: 10.1029/2022JE007291.
- Frédéric Schmidt, Michael J. Way, François Costard, Sylvain Bouley, Antoine Séjourné, and Igor Aleinov. Circumpolar ocean stability on Mars 3 Gy ago. *Proceedings of the National Academy of Science*, 119(4):e2112930118, January 2022. doi: 10.1073/pnas.2112930118.
- P. Kenneth Seidelmann and S. E. Urban. *Explanatory Supplement to the Astronomical Almanac, Third Edition*. 2013. ISBN 978-1-891389-85-6.

Eite Tiesinga, Peter J. Mohr, David B. Newell, and Barry N. Taylor. CODATA recommended values of the fundamental physical constants: 2018. *Reviews of Modern Physics*, 93:025010, Jun 2021. doi: 10.1103/RevModPhys.93.025010. URL <https://link.aps.org/doi/10.1103/RevModPhys.93.025010>.

J. Touma and J. Wisdom. The Chaotic Obliquity of Mars. *Science*, 259(5099):1294–1297, February 1993. doi: 10.1126/science.259.5099.1294.

Michaela Walterová, Marie Běhounková, and Michael Efroimsky. Is There a Semi-Molten Layer at the Base of the Lunar Mantle? *Journal of Geophysical Research (Planets)*, 128(7):e2022JE007652, 2023. doi: 10.1029/2022JE007652.

William R. Ward and Mark J. Reid. Solar tidal friction and satellite loss. *Monthly Notes of the Royal Society*, 164:21, 1973. doi: 10.1093/mnras/164.1.21.